CHAPTER IV

RESULTS AND DISCUSSION

4.1 Grafting of NR with MMA

The graft copolymerization of NR latex with MMA was proceeded using conc. Latex with high ammonia preserved NR latex with 30% DRC, which was diluted from initially 60% DRC by 0.7% ammonia solution. During the grafting process, potassium hydroxide solution (10%w/v) was added to the latex in order to maintain the basic pH as well as the latex stability. An emulsifying agent, SDS was also added with gentle stirring to prevent foaming in order to provide colloidal stability of the latex [18]. The grafting process took place by the MMA monomer that was absorbed on the surface of latex particles. Then CHPO/TEPA, the oil-soluble peroxide and the water-soluble reductant, generated radicals at the NR–water interface, facilitating the polymerization of the MMA at the interface [15]. This led to the formation of a PMMA layer around the seed NR particle as observed by TEM analysis shown in Figure 4.1. The shape of ruthenium-stained NR particles in the latex appeared to be spherical (Figure 4.2 (a)). After the grafting process, a semi-transparent layer covering the seed particle was obtained. The grafted NR particles shows a core–shell structure (Figures 4.2 (b)) because the Ru-staining occured exclusively at the unsaturated double bonds (C=C) of the NR. PMMA was not stained very well and appeared as semi-transparent object in the micrograph. This evidence suggests that the grafted polymers taking place at the surface of the NR particle in the latex to give an PMMA shell layer.

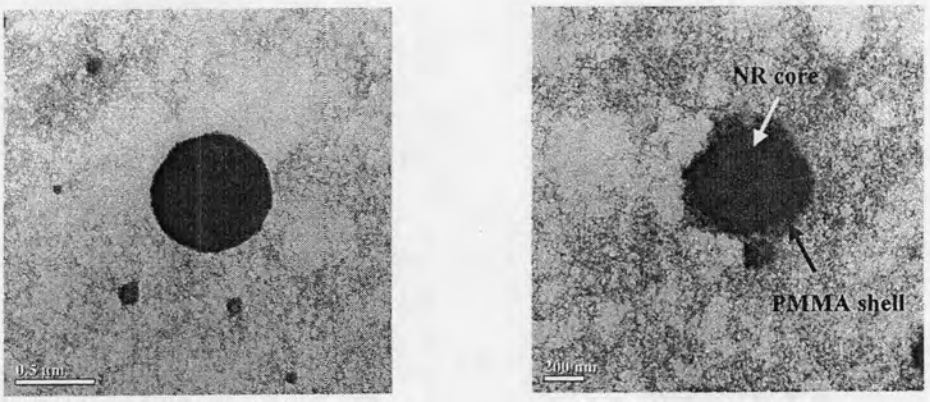

(a) (b)

Figure 4.1 Comparison of the transmission electron micrographs of (a) NR and (b) NR-*g*-MMA.

The grafting efficiency of NR with MMA was studied at a fixed weight ratio of 85:17.65 in phr, and the reaction temperature at 50°C, with varied reaction time at 1, 3, and 6 hr. The amount of graft copolymer and homopolymers formed during the grafting step was analyzed. When the reaction time was increased, no marked difference was observed for the percentages of monomer conversion, graft copolymer, free homopolymer, and grafting efficiency (Table 4.1). Basically, conversion of MMA monomer to graft onto rubber particles should increase with increasing the reaction time or at least having a constant conversion [18]. Thus, 1 hr grafting time was chosen for the graft copolymerization of NR with MMA.

Table 4.1 Grafting efficiency of NR latex with MMA

Raction time (h)	Monomer conversion (%)	Grafted NR (%)	Free homopolymer (%)		GE (%)
			NR	PMMA	
1	95.83	75.35	20.62	4.02	65.08
3	95.45	75.31	20.63	4.01	64.63
6	95.03	73.79	22.07	4.03	62.82

After soxhlet extraction of the NR-*g*-MMA, the grafted NR was analyzed for its functional groups by FTIR technique (Figure 4.2). The FTIR spectra of NR show the absorption bands of the aliphatic C-H stretching vibration at 2950 cm^{-1}, the C-C stretching vibration at 1239 cm^{-1} and 1372 cm^{-1}, and the C=C stretching vibration at 830 cm^{-1} [44]. Two distinct new peaks in the IR spectra of the grafted NR were found at 1736 and 1137 cm^{-1}, corresponding to the C=O and C-O-C groups in the methacrylate of MMA [45]. This confirms the grafting of MMA on the NR latex.

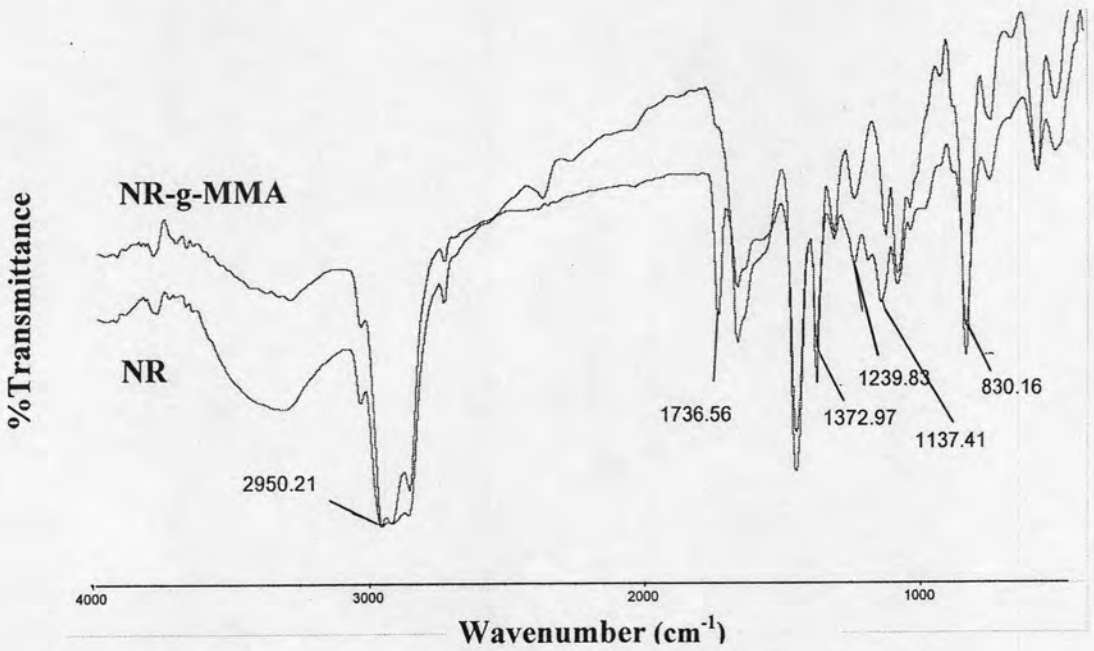

Figure 4.2 Comparison between the FTIR spectra of NR and NR-*g*-MMA.

In the SEM micrograph, the cryogenically fractured surface of NR-*g*-MMA is evidently rougher than the surface of NR film, as shown in Figure 4.3 (a) and (b). The surface roughness increased with increasing PMMA content [1]. The stiffer MMA, as compared to NR, tended to aggregate and became globular in shape [3].

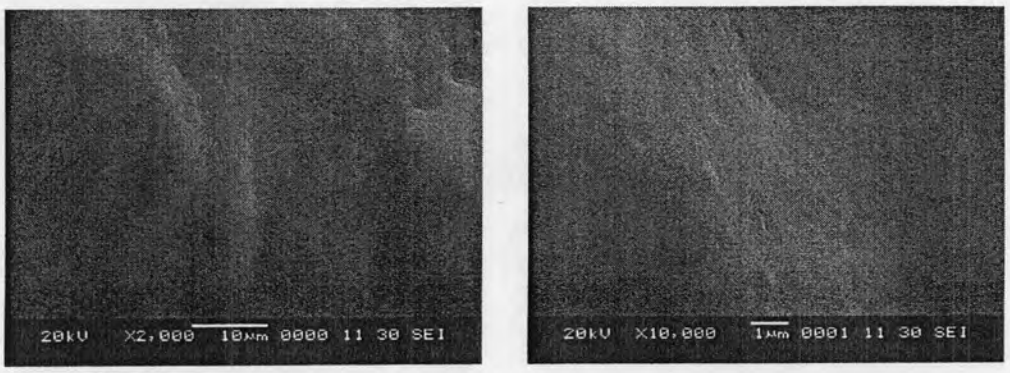

(a)

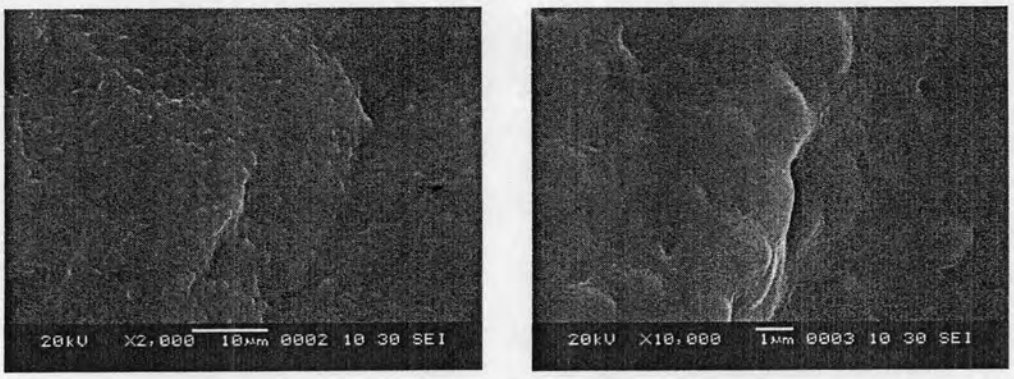

(b)

Figure 4.3 Comparison of the fractured surfaces of (a) NR and (b) NR-*g*-MMA film by SEM.

In addition, the fractured surfaces of NR and NR-*g*-MMA cast films were analyzed for elements in the graft copolymer at a selected area of the rubber matrix by EDX technique. In Figure 4.4 (a) and (b), the SEM-EDX spectra indicate clearly the C and O peaks on the fractured surface.

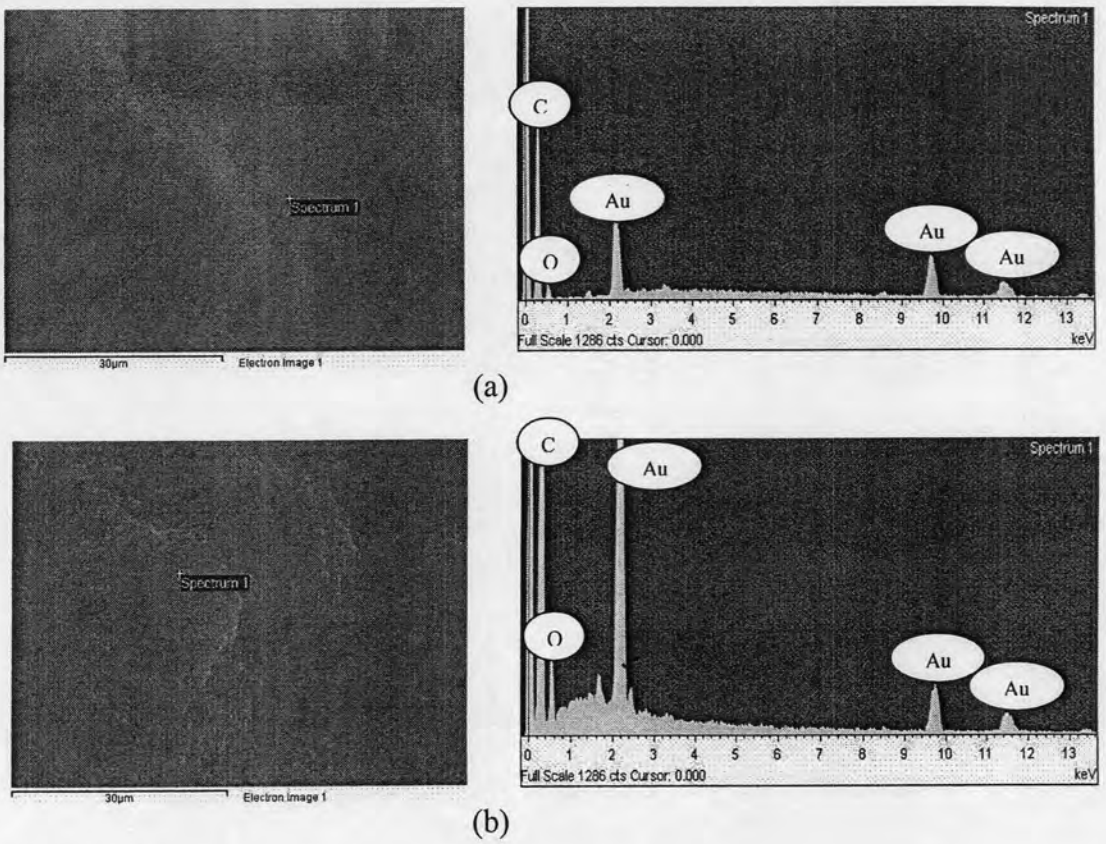

Figure 4.4 EDX spectra of (a) NR and (b) NR-*g*-MMA.

4.2 Grafting of NR-*g*-MMA with γ-MPS

A silane coupling agent, γ-MPS, is capable of providing chemical bonding between an organic material and inorganic material. The vinyl group in γ-MPS (Figure 2.7), should be reactive towards the unsaturated NR chains and the MMA radical chain end, while the other reactive group, methoxysilyl group, can form siloxane bond (Si-O-Si) with other alkoxysilane molecules, i.e. TEOS and/or other γ-MPS molecules.

In this work, graft copolymerization between NR and MMA was firstly prepared. Then the addition of γ-MPS was performed with the goal to graft γ-MPS on the NR-*g*-MMA particles in the latex.

4.2.1 Latex stability

The influence of γ-MPS on the colloidal stability in the emulsion polymerization was investigated by changing the mixing order of each chemical in the latex compound during the grafting process. Five formulations are given in Table 3.1. The latex compound in formulation 1 was prepared by adding γ-MPS after MMA was added at room temperature. After 15 min stirring, the initiator was then added to the latex to initiate the grafting of both MMA and γ-MPS simultaneously. The mixed latex unfortunately began to coagulate after adding the initiator for 20 min, indicating that stable latex could not be obtained. The coagulation was most likely caused by premature hydrolysis/condensation of the methoxy silyl group in γ-MPS. In formulation 2, γ-MPS was added after the MMA grafting step. The latex compound obtained in the formula 2 was fairly stable but, in the SEM micrographs, the *in situ* generated silica particles were found at the bottom portion of the composite film. This suggested that silica particles were formed very fast, before the latex film was formed. It was also possible that γ-MPS was not efficiently grafted on the latex particles. To solve this problem, formulations 3 was prepared by the addition of the 2nd portion of the initiator into the system after the MMA grafting step. In addition, in the formulations 3, the reaction time of γ-MPS grafting was reduced to 15 min in order to avoid prolonged contact with water at 50°C. It was, however, found that coagulum formed after the second initiator dose was added and stirred for 15 min. Luo et al. [46] studied the consumption rate of monomer in the copolymerization of MMA/γ-MPS and found that γ-MPS was consumed slowly into the polymer chain. On the other hand, the methoxy end of γ-MPS proceeded with the hydrolysis and condensation of γ-MPS units to form the siloxane bond, leading to latex coagulation.

From formulations 1-3, it can be seen that the reaction temperature and time are the important factors affecting latex stability. In formulation 4, γ-MPS was added to the compound after the second dose of the initiator was added at room temperature for 15 min. This successfully prevented the coagulation and increased the probability of γ-MPS grafting. When comparing γ-MPS with TEOS, the methoxysilane groups in γ-MPS have shorter steric hindrance than the ethoxysilane groups in TEOS, it is

supposed that γ-MPS should be susceptible to hydrolysis more than TEOS [7]. To avoid premature coagulum, a short reaction time (ca.15 min) and a low (room) temperature were chosen to prepare the NR-*g*-MMA-γ-MPS latex compound. Thus, the optimal polymerization condition for obtaining the latex compound with good stability is the formulation 4.

4.2.2 Silica formation in NR-*g*-MMA-γ-MPS

The NR-*g*-MMA-γ-MPS and NR-*g*-γ-MPS particles were studied by TEM whose results are shown in Figure 4.5 (a) and (b), respectively. For NR-*g*-MMA-γ-MPS, dark-shaded silica nanoparticles grow radially outward from the seed latex particle giving the silica-coated NR-*g*-MMA particles with a core-shell morphology (Figure 4.5 (a)). The NR-*g*-γ-MPS also gives NR core and surrounding silica shell (Figure 4.5 (b)). In addition, small and dark particles are seen widely dispersed in the emulsion phase (Figure 4.5 (c)). These dispersed particles probably are the ungrafted γ-MPS homopolymer particles [35]. These results indicate that γ-MPS can undergo sol-gel process to create *in situ* alkylated silica at either the rubber shell by grafting or copolymerization with NR-*g*-MMA latex particles or remaining in the continuous phase in the form of low molecular weight cyclic oligomers.

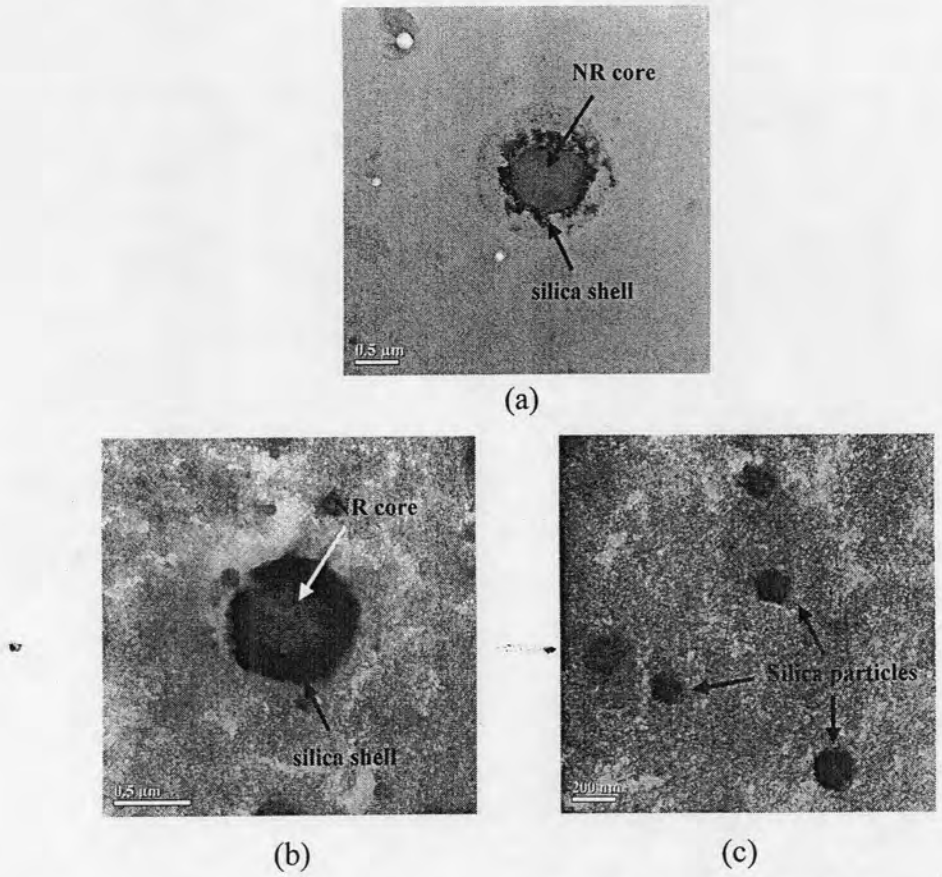

Figure 4.5 Transmission electron micrographs of (a) NR-*g*-MMA-γ-MPS2, (b) NR-*g*-γ-MPS2 and (c) unbound silica particles found in NR-*g*-γ-MPS2.

The content and the percentage of conversion of silica in the silica/NR-*g*-MMA composite films are listed in Table 4.2. The silica contents generated in the composites increase with increasing γ-MPS loading, since γ-MPS also provided the *in situ* silica. It is however found that the total conversion of γ-MPS slightly decreases when increasing the added content of γ-MPS. This is likely because the increase in the steric bulkiness of the organic substituent in the γ-MPS has an inhibitory effect on the hydrolysis and condensation reaction during the sol-gel process.

Table 4.2 The silica content and percentage of γ-MPS conversion to silica

Sample	γ-MPS (phr)	Silica (theoretical) (phr)	Silica (experimental) (phr)	%Conversion
NR-*g*-MMA	0.00	0.00	0.00	0
NR-*g*-MMA-γ-MPS1	1.76	0.77	0.69±0.08	89
NR-*g*-MMA-γ-MPS2	3.53	1.55	1.12±0.16	72

The fractured surfaces of the *in situ* silica/NR-*g*-MMA composites were analyzed by SEM (Figure 4.6). Silica particles in the NR-*g*-MMA-γ-MPS1 and NR-*g*-MMA-γ-MPS2 composite which contains 1.76 and 3.53 phr of γ-MPS are shown in Figure 4.6 (a) and (b) respectively.

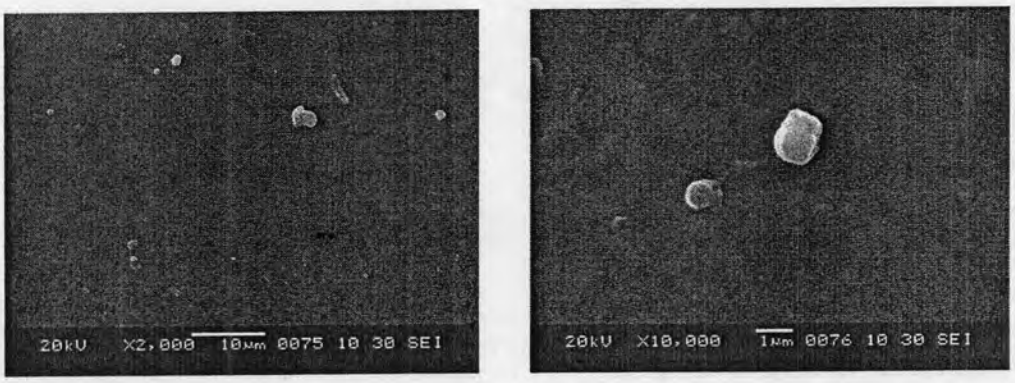

(a)

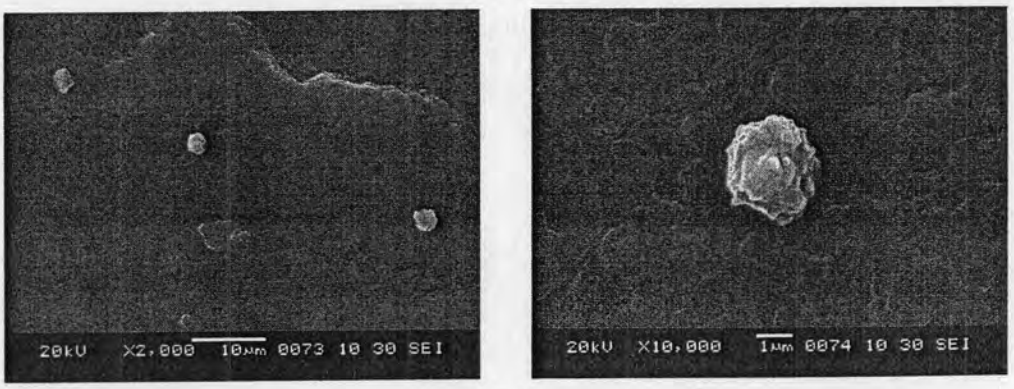

(b)

Figure 4.6 Scanning electron micrographs of (a) NR-*g*-MMA-γ-MPS1 (1.76 phr of γ-MPS) and (b) NR-*g*-MMA-γ-MPS2 (3.53 phr of γ-MPS).

4.2.3 Grafting efficiency of γ-MPS

NR-*g*-γ-MPS was subjected to soxhlet extraction by petroleum ether. It was found that 11.48%wt of free NR was removed from the composite. This suggests that upto 88.52%wt of γ-MPS grafted NR is present in the results composites. Moreover, NR-*g*-MMA-γ-MPS was also purified by soxhlet extraction by petroleum ether. It was found that 10.66%wt of free NR was removed from the composite, indicating that upto 89.34%wt of NR could be grafted by γ-MPS. The soxhlet extraction using acetone could not be used to extract the free poly (γ-MPS) or γ-MPS monomer out of the composite, because the silane was transformed to silica which could not be extracted by any organic solvents.

4.3 *In situ* formation of silica from TEOS and γ-MPS in the grafted NR composites

In the preparation of *in situ* silica of NR-*g*-MMA-γ-MPS, the parameters affecting the silica formation in NR-*g*-MMA-γ-MPS were investigated and discussed as follows.

4.3.1 General observation

The appearances of the composite films prepared in this study are shown in Figure 4.7. The NR-*g*-MMA latex gave transparent films with yellowish color (Figure 4.7 (a)). When TEOS was added to the latex compound, the obtained composite films turned opaque due to the silica particles. The composite films were prepared from 15 phr TEOS and 3.53 phr γ-MPS, thus TEOS transformed to silica in a higher content than did the γ-MPS. Therefore, the NR-*g*-MMA-TEOS and NR-*g*-MMA-γ-MPS-TEOS film (Figure 4.7 (b) and (d)) were more opaque than the NR-*g*-MMA-γ-MPS film (Figue 4.7 (c)). No loosely bound silica was observed on the composite film.

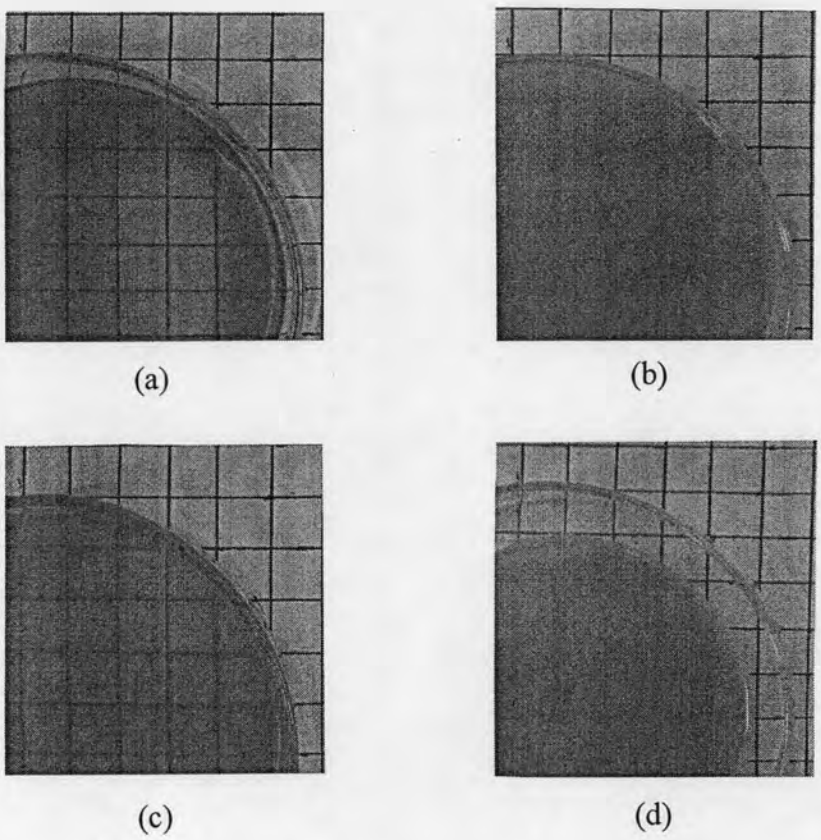

Figure 4.7 Photographs of (a) NR-*g*-MMA, (b) NR-*g*-MMA-TEOS15, (c) NR-*g*-MMA-γ-MPS2, (d) NR-*g*-MMA-γ-MPS2-TEOS15.

4.3.2 Effect of heating time on silica formation in the latex compound

From previous studies, the sol-gel process of TEOS occurred during the heating step at 50°C [3,6,32,47]. Two major ingredients required for the sol-gel process, i.e. water and ammonia as the base catalyst, were present in the latex. It was therefore worth exploring the effect of heating time on the content of silica generated from both TEOS and γ-MPS in the composites. The composite being investigated was prepared from the latex mixture with NR:MMA:γ-MPS:TEOS weight ratio of 85:14.12:3.53:15.

The silica contents in the NR-*g*-MMA-γ-MPS-TEOS composites obtained by the sol-gel process of γ-MPS and TEOS after varying the heating times at 50°C are shown in Figure 4.8. It was found that the amount of silica generated in the composite

increased after just one day of heating and remained unchanged after 2 days. The heating period was therefore set at 2 days for the preparation of the composites in this study.

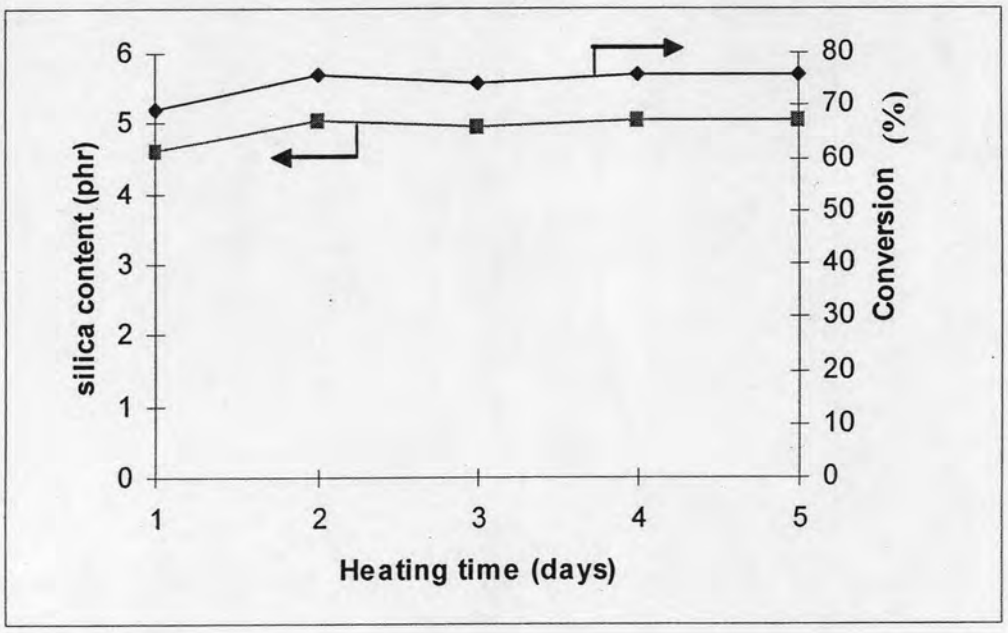

Figure 4.8 Changes of silica content and %conversion of γ-MPS/TEOS to silica as a function of heating time for the *in situ* silica/NR-*g*-MMA-γ-MPS composites at 50°C.

4.3.3 FT-IR Spectroscopy analysis of the *in situ* silica

FT-IR analysis results of silica/NR composites are shown in Figure 4.9. The FTIR spectra of NR exhibit the characteristic transmission peaks at 3035, 2960 and 834 cm^{-1} corresponding to the stretching vibration of olefinic =C–H, stretching vibration of –C–H and out-of-plane bending, vibration of aliphatic =C–H, respectively. Strong bands at 1730 cm^{-1} and 1145 cm^{-1} are attributed to the C=O stretching and C-O-C stretching of MMA which was grafted on the NR backbone. The silica generated in the composites exhibits IR peaks at 1100–1040 cm^{-1}, assigning to the Si–O–Si bridging bonds in Figure 4.9 (c-g). Those FT-IR results also confirm the existence of silica in the composite films [48].

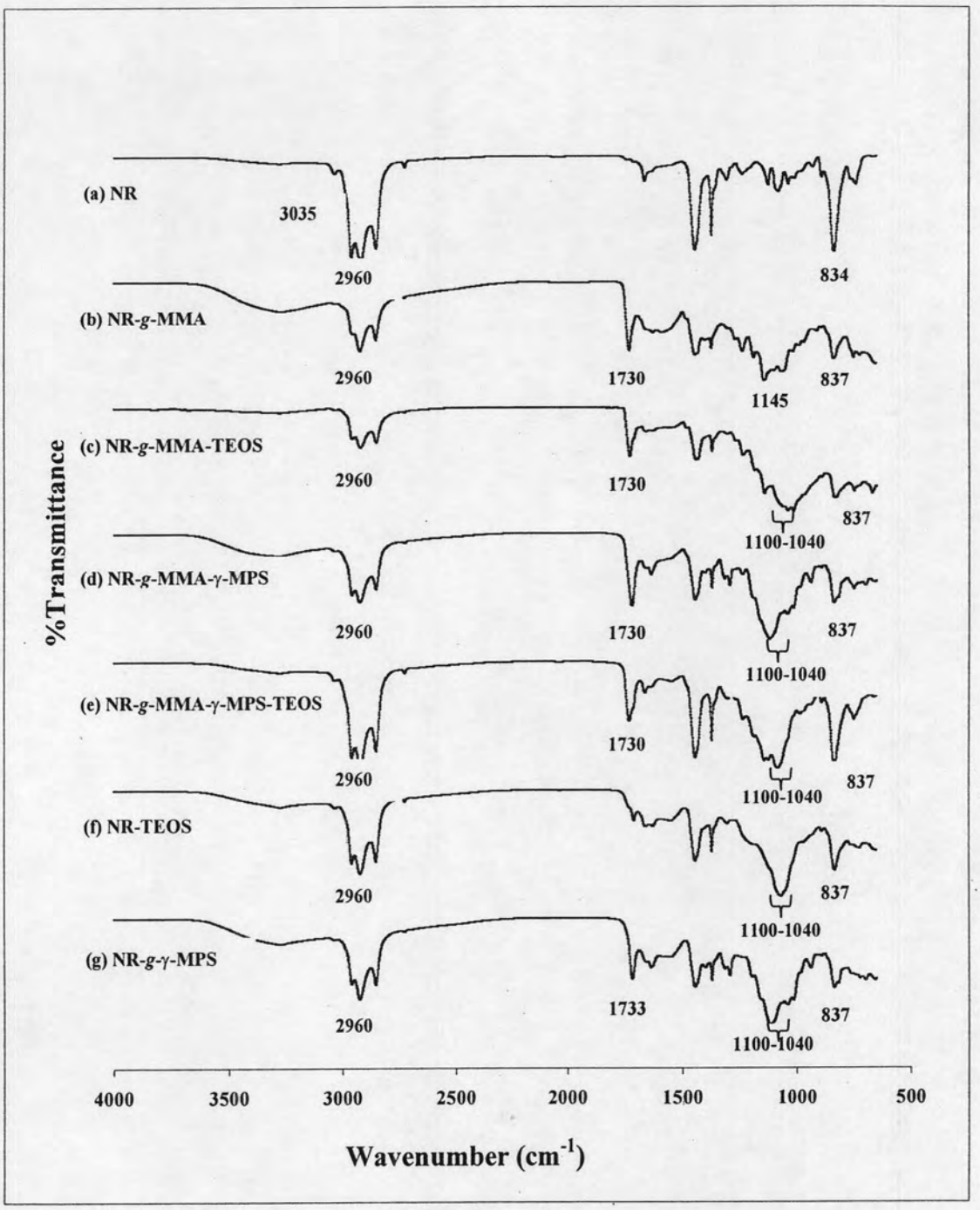

Figure 4.9 FT-IR spectra of (a) NR, (b) NR-*g*-MMA, (c) NR-*g*-MMA-TEOS, (d) NR-*g*-MMA-γ-MPS, (e) NR-*g*-MMA-γ-MPS-TEOS, (f) NR-TEOS, and (g) NR-*g*-γ-MPS.

4.3.4 Morphological investigation of the *in situ* silica composites

The latexes of NR-*g*-MMA-TEOS15, NR-*g*-MMA-γ-MPS2-TEOS15 and NR-TEOS15 were characterized by TEM (Figure 4.10). The TEM image clearly shows dark areas of silica coated the grafted or ungrafted NR as a core shell morphology (Figure 4.10 (a-c)). Polycondensation of the silane was promoted by a high local TEOS concentration and γ-MPS introduced on the latex surface and/or possibly into the hybrid latex core [35]. Indeed, due to its hydrophobic character, TEOS can easily enter the polymer particles, but only at the rubber latex surface that TEOS can react with water and hydroxide ion. In addition, free-standing relative dark polysiloxane clusters which accumulate in water was observed in the NR-TEOS sample (Figure 4.10 (d)). This suggests that the unbound TEOS is also present in the colloid.

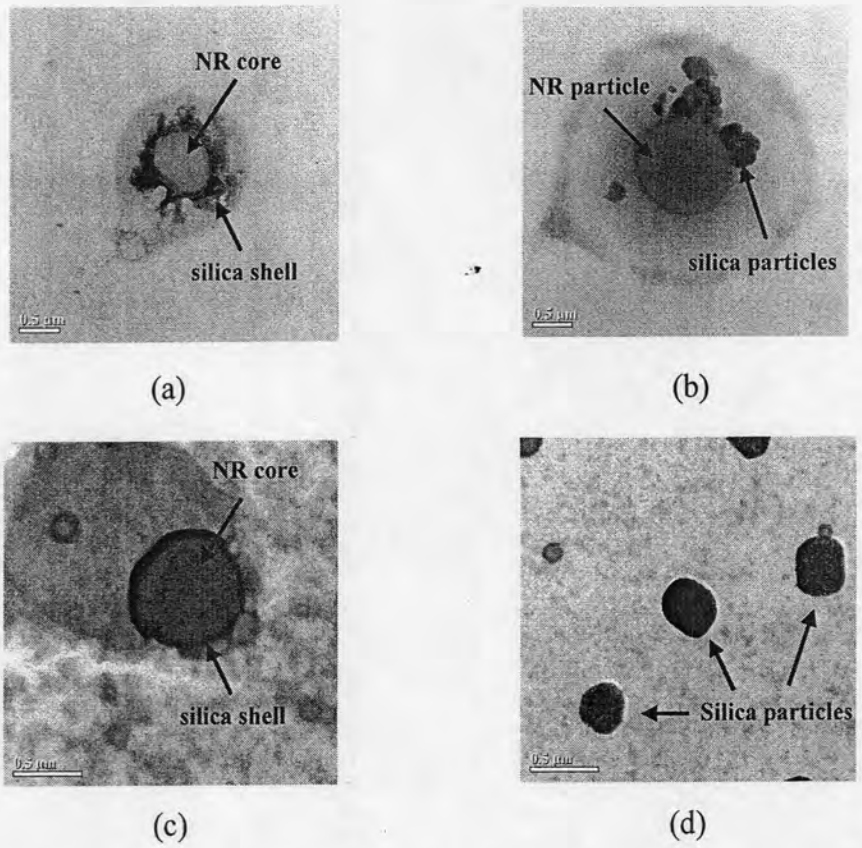

Figure 4.10 Transmission electron micrograph of (a) NR-*g*-MMA-TEOS15, (b) NR-*g*-MMA-γ-MPS2-TEOS15, (c) NR-TEOS15, and (d) silica particles of unbound TEOS found in NR-TEOS sample.

4.3.5 Content of *in situ* silica

The silica content and % conversion of γ-MPS and TEOS to silica in the grafted NR latexes are shown in Table 4.3. It was found that the *in situ* silica content increased with increasing added TEOS amount from 5 to 15 phr. TEOS underwent hydrolysis and condensation to form silica at an average conversion of 90%. Because the TEOS molecule contains four ethoxy groups, therefore undergoing sol-gel process to form silica almost completely as found in earlier reports [6]. Moreover, if the mixing time (at room temperature) was too short, the liquid TEOS was not homogeneously mixed with the latex. If the mixing time was too long, TEOS could evaporate. It could result in a low amount of the *in situ* silica. In the case of γ-MPS mixed with the latex compound, the %conversion of the generated silica in the composite decreased when increasing the amount of γ-MPS as found and discussed in section 4.22 and Table 4.2.

Table 4.3 The silica content and percentage of conversion of γ-MPS and TEOS to silica

Sample	γ-MPS (phr)	Silica (theoretical) (phr)	Silica (experimental) (phr)	%Conversion
NR-*g*-MMA-TEOS5	0.00	1.70	1.58±0.16	93
NR-*g*-MMA-TEOS10	0.00	3.39	3.08±0.07	91
NR-*g*-MMA-TEOS15	0.00	5.09	5.09±0.18	85
NR-*g*-MMA-γ-MPS1-TEOS5	1.76	2.47	2.24±0.19	90
NR-*g*-MMA-γ-MPS1-TEOS10	1.76	4.17	3.71±0.13	89
NR-*g*-MMA-γ-MPS1-TEOS15	1.76	5.86	4.67±0.15	80
NR-*g*-MMA-γ-MPS2-TEOS5	3.53	3.25	2.10±0.08	65
NR-*g*-MMA-γ-MPS2-TEOS10	3.53	4.94	3.13±0.12	63
NR-*g*-MMA-γ-MPS2-TEOS15	3.53	6.64	4.14±0.16	62

4.3.6 Scanning electron micrographs (SEM)

The fractured surfaces of the NR-*g*-MMA-TEOS and NR-*g*-MMA-γ-MPS-TEOS composites were analyzed by SEM (Figure 4.11). In the NR-*g*-MMA-TEOS composites, the silica generated from TEOS tended to agglomerate and formed clusters having various sizes (Figure 4.11 (a-c)). It has a rather low interaction between silica from TEOS and NR-*g*-MMA, but a strong silica–silica interaction by hydrogen bonding resulted in the observed neighboring silica aggregations [9]. There was a report suggesting that the particle size was increased by increasing the amounts of the silica precursor (TEOS) [41]. When the composite was treated with γ-MPS (Figure 4.11 (d-i)), which was used as a silane coupling agent, it was observed that the silica particle size from γ-MPS/TEOS was averagely smaller than the silica from TEOS alone. In addition, increasing the amount of γ-MPS led to an increase of silica particle sizes as seen in Figure 4.11 (g-i). This result suggests that the use of γ-MPS is able to prevent particle aggregation. The methacryloyl group on γ-MPS possibly provides a chemical link between the NR and silica via the grafted MMA chains. The addition of silane coupling agent provides a better filler dispersion due to the significant reduction of filler–filler interaction [34].

Both TEOS and γ-MPS undergo hydrolysis to generate silanol groups. These then condense to form Si-O-Si linkages. However, hydrolysis and condensation can, and most likely do, take place simultaneously [49]. For the mixed-precursor system, the complexity arise not only for statistically possible cross reactions of different silanes but also for changes that happens in the reaction kinetics of the individual silane compounds when the system changes from a single-precursor to a mixed-precursor system [48].

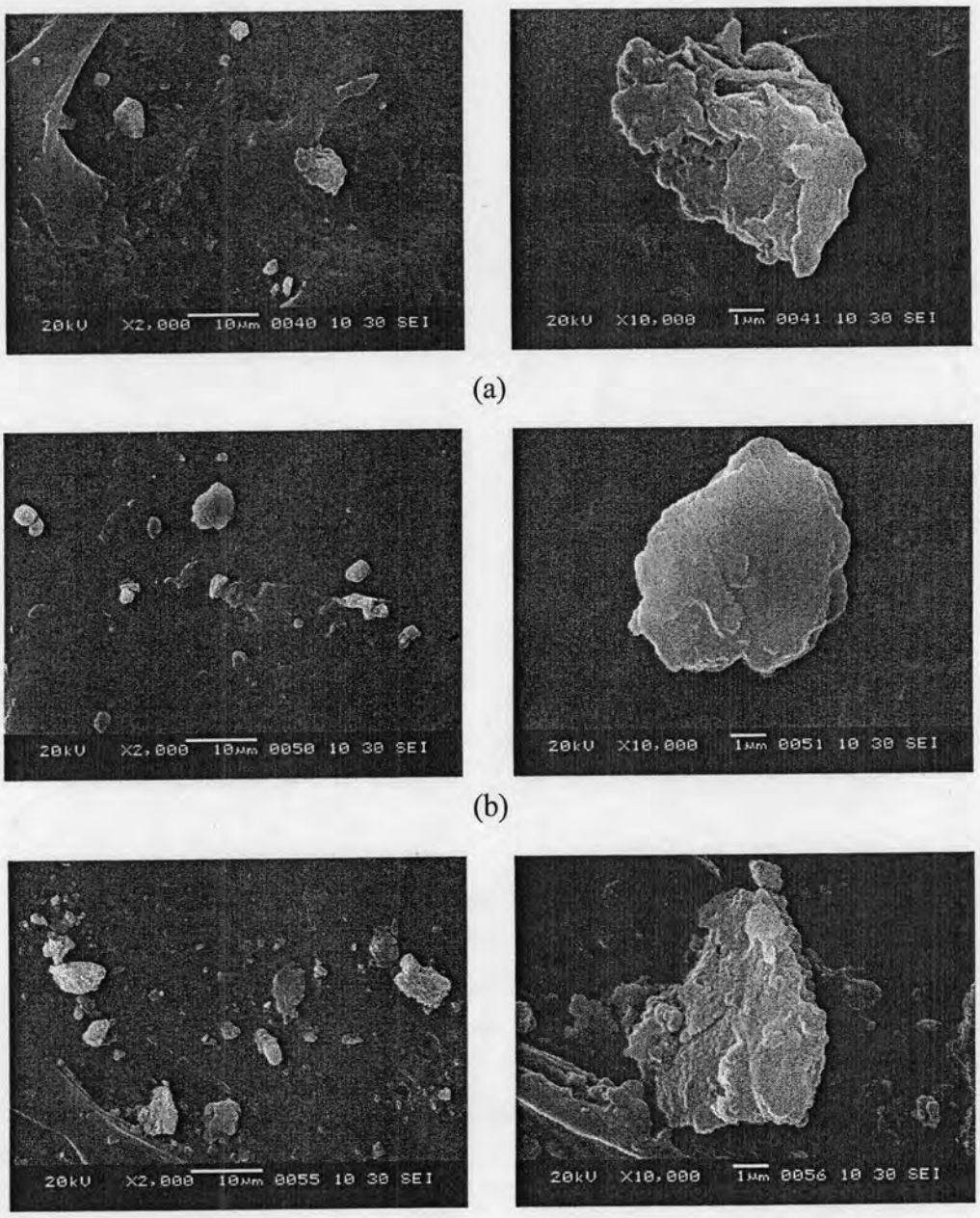

Figure 4.11 Scanning electron micrographs of the composite films: (a) NR-*g*-MMA-TEOS5, (b) NR-*g*-MMA-TEOS10, (c) NR-*g*-MMA-TEOS15.

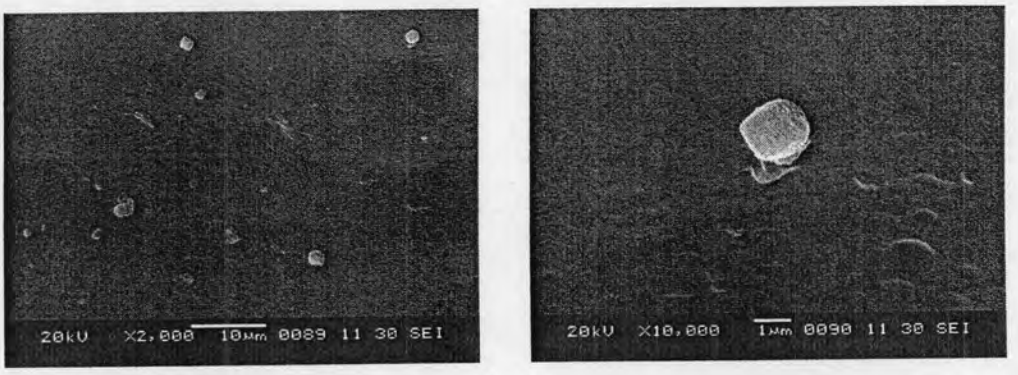

(d)

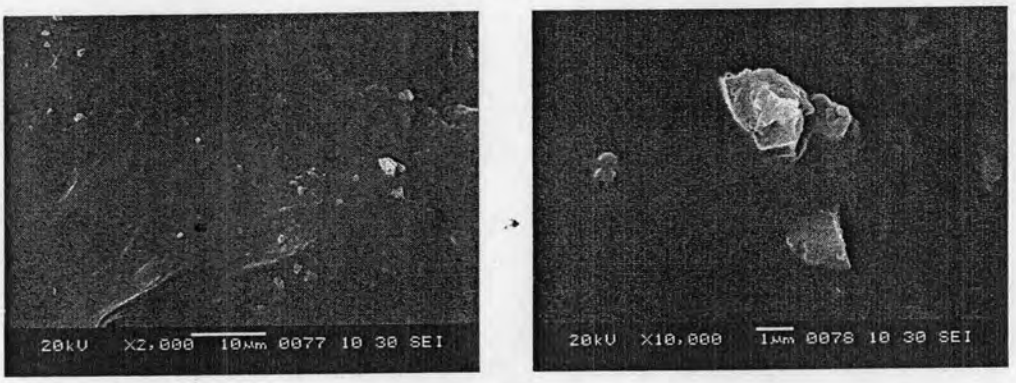

(e)

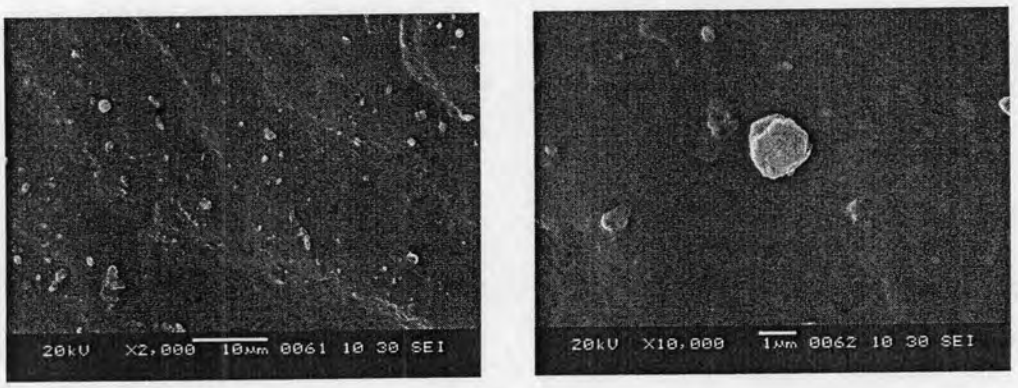

(f)

Figure 4.11 Continued scanning electron micrographs of the composite films: (d) NR-*g*-MMA-γ-MPS1-TEOS5, (e) NR-*g*-MMA-γ-MPS1-TEOS10, (f) NR-*g*-MMA-γ-MPS1-TEOS15.

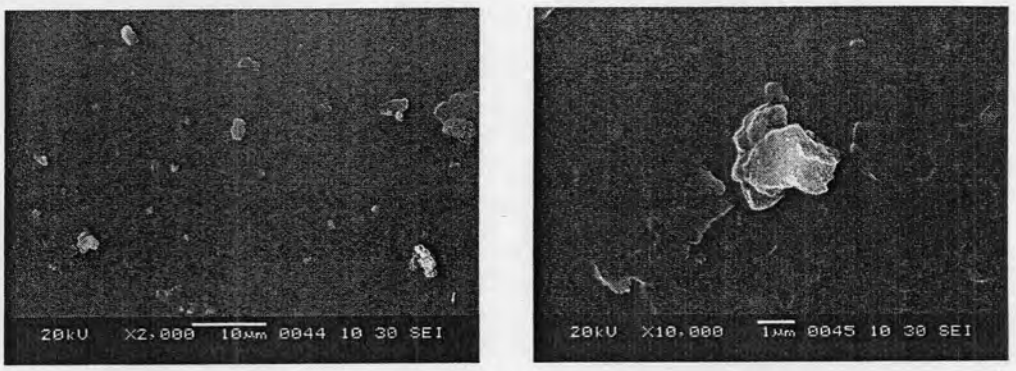

(g)

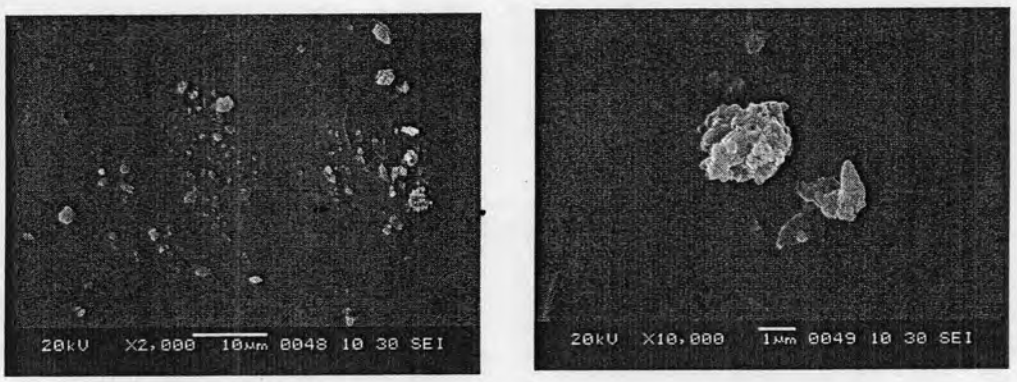

(h)

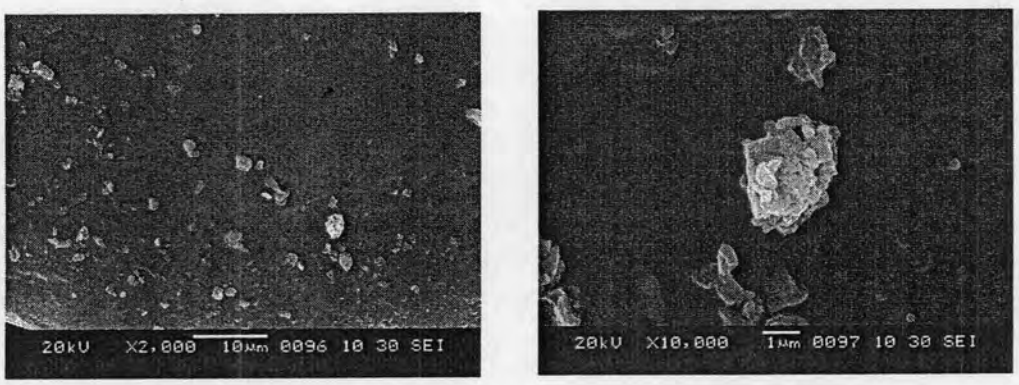

(i)

Figure 4.11 Continued scanning electron micrographs of the composite films: (g) NR-*g*-MMA-γ-MPS2-TEOS5, (h) NR-*g*-MMA-γ-MPS2-TEOS10, (i) NR-*g*-MMA-γ-MPS2-TEOS15.

The SEM-EDX method was to identify atomic types on the cross-sectioned surface of *in situ* silica incorporated NR-*g*-MMA-γ-MPS films (Figure 4.12). The SEM-EDX spectrum shows a strong peak of Si atom on the fractured surface at 1.75 keV. This results confirms the silica (~ 6 phr) formation inside the rubber matrix. These results therefore indicate that silica particles are successfully generated in the composite films.

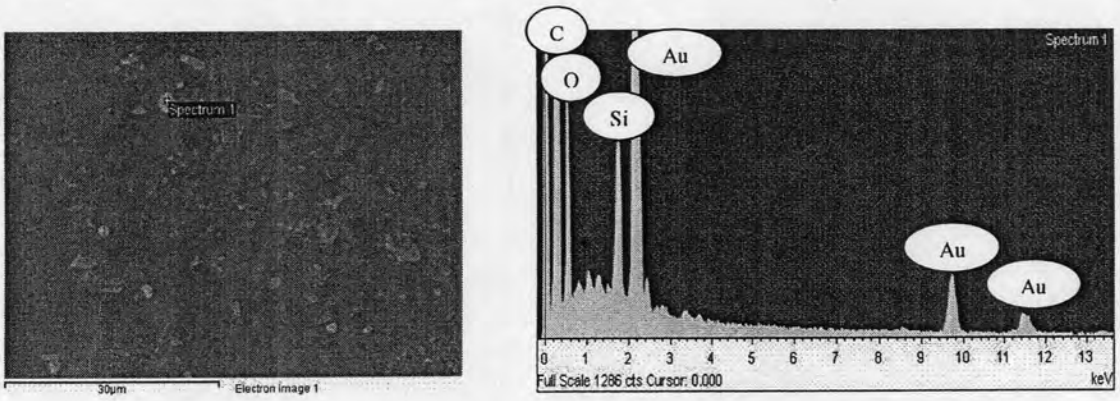

Figure 4.12 EDX spectra of NR-*g*-MMA-γ-MPS-TEOS

4.3.7 Solid-state ^{29}Si NMR analysis

Solid-state ^{29}Si cross-polarization magic angle spinning (CPMAS) NMR experiment was to identify the local environments of the silicon atoms in the composite materials, as also reported by Han et al. [50]. The NMR spectra of the NR-*g*-MMA-γ-MPS and NR-*g*-MMA-γ-MPS-TEOS composites are shown in Figure 4.13. A Q species is the one in which the Si atom is capable of producing four siloxane bonds, whereas a T species is belong to a Si atom connecting to three siloxane bonds, such as a silane which has a single R′ group directly bonded to a Si atom. Therefore, if there are complete hydrolysis and condensation reactions of silane as a final result, only T^3 and Q^4 species will be detected in the ^{29}Si NMR spectra.

Table 4.4 Designation of the various structural units of silicon atoms in TEOS and γ-MPS [50]

T species			Q species			
T^1	T^2	T^3	Q^1	Q^2	Q^3	Q^4
Structural units of silicon atoms						
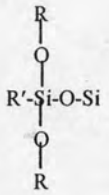	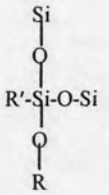	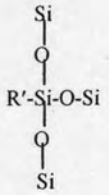		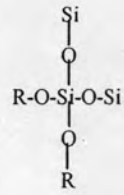	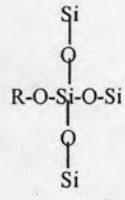	

R is an H or an alkyl group and R′ is an alkyl or a $(CH_2)X$ group.

The NMR spectra of NR-*g*-MMA-γ-MPS composite (Figure 4.13 (a)) show two signal at approximately -60 ppm, corresponding to the T^2 species and the signal at approximately -67 ppm, corresponding to the T^3 species. The NMR spectra of NR-*g*-MMA-γ-MPS-TEOS composite (Figure 4.13 (b)) show four signals -60 ppm corresponding to the T^2 species, -67 ppm corresponding to the T^3 species, at -102 ppm, corresponding to the Q^3 species, and also the Q^4 signal at -111 ppm. No T^1 peak was found in the NMR spectra, indicating that all γ-MPS in the starting compositions have participated in the condensation reaction. These results indicate that the hydrolysis and condensation reaction of γ-MPS and TEOS have transformed to silica and/or alkylated silica in the NR-*g*-MMA-γ-MPS and NR-*g*-MMA-γ-MPS-TEOS composites.

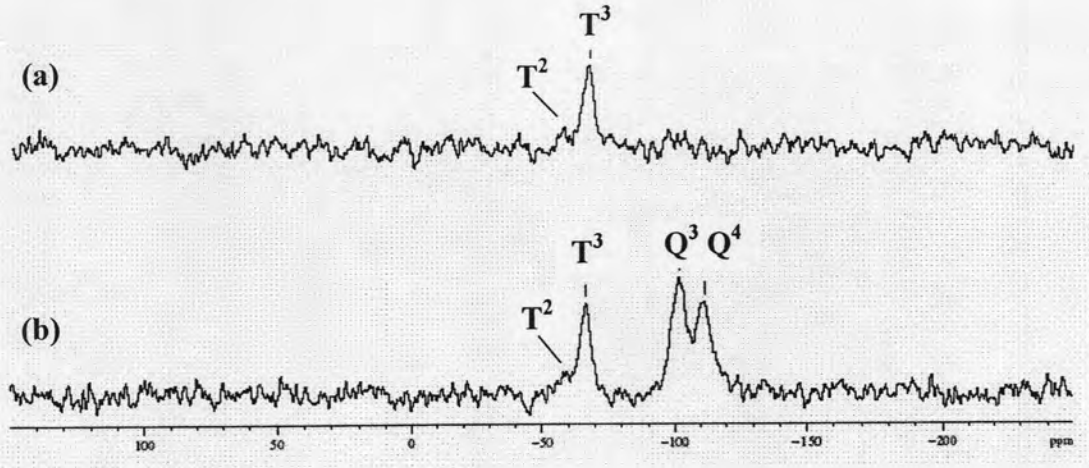

Figure 4.13 ^{29}Si CP/MAS NMR spectra of (a) NR-*g*-MMA-γ-MPS2 (b) NR-*g*-MMA-γ-MPS2-TEOS15.

4.4 Swelling behaviour

The degree of swelling of NR and silica/grafted NR films in toluene are shown in Figure 4.14. The effect of *in situ* silica contents on the swelling behaviour was invertigated. The swelling behaviour of the silica/grafted NR films decreased with increasing contents of *in situ* silica. This is because chain motions of rubber in the silica/grafted NR films become restricted by silica particles.

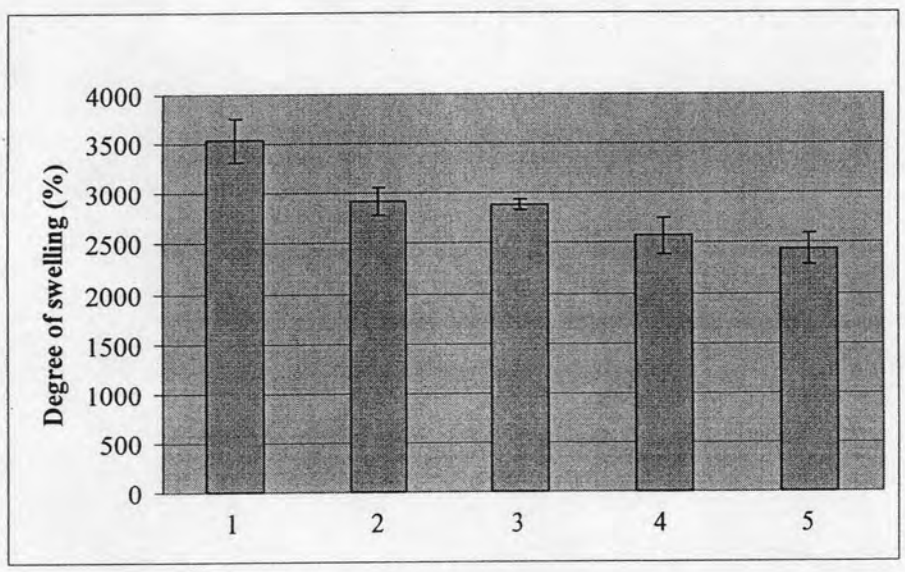

Figure 4.14 Degree of swelling of the (1) NR, (2) NR-*g*-MMA, (3) NR-*g*-MMA-γ-MPS, (4) NR-*g*-MMA-TEOS and (5) NR-*g*-MMA-γ-MPS-TEOS composite films.

4.5 Thermal properties

The glass transition temperatures (T_g) of the rubber composites are shown in Figure 4.15 and Table 4.5. The T_g of the uncrosslinked neat NR was reportedly at -72°C [51], whereas the T_g's of NR-*g*-MMA was found at -68.5°C. The γ-MPS and/or TEOS containing composites showed two T_g's, -68.4 and -10.2°C for NR-*g*-MMA-γ-MPS, -67.3 and -11.0°C for NR-*g*-MMA-TEOS, and -67.9 and -11.3.0°C for NR-*g*-MMA-γ-MPS-TEOS. The second transition temperature of each composite could be possible ascribed to the dipole-dipole interactions between the silica particles and the polar group in NR molecules. The observed transition might be due to the relaxation of tightly bound silica by the NR matrix. Although the amounts of MMA and the generated silica inside NR were not high, their T_g's were shifted to slightly higher temperatures. It may be assumed that the thermal stability of organic materials can be improved by introducing inorganic components such as silica, on the basis of the fact that these materials have inherently good thermal stability [52,53].

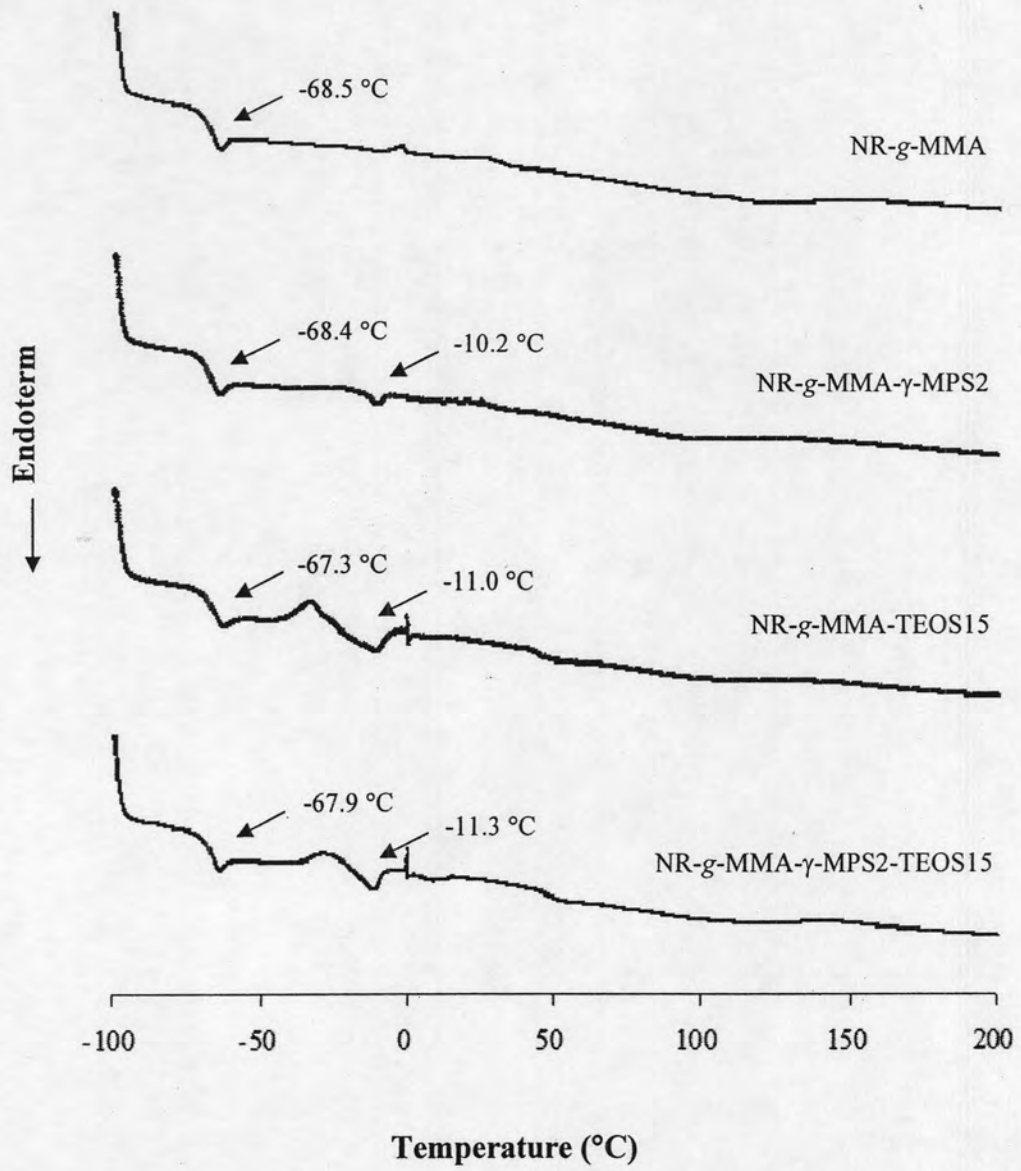

Figure 4.15 DSC curves of the NR-*g*-MMA and the generated silica inside the NR-*g*-MMA.

Table 4.5 Glass transition temperature of the composite films

Sample	NR:MMA: γ-MPS (phr)	TEOS (phr)	T_{g1} (°C)	T_{g2} (°C)
NR-*g*-MMA	85:17.65:0	-	-68.5	-
NR-*g*-MMA-γ-MPS2	85:14.12: 3.53	-	-68.4	-10.2
NR-*g*-MMA-TEOS15	85:17.65:0	15	-67.3	-11.0
NR-*g*-MMA-γ-MPS2-TEOS15	85:14.12:3.53	15	-67.9	-11.3

The thermal stability of the *in situ* silica/NR-*g*-MMA composites studied by TGA in air are shown in Figure 4.16. The air oxidative degradation of films took place in two steps. The first step obtained from rubber decomposition is in the temperature range of 300-450°C and accounting for about 90% of mass. This first step of thermal oxidation degradation is attributed to the organic part of NR and grafted portion. The second step of degradation was between 450-600°C accounting for 6% mass, which related to the degradation of crosslink in the composites. In addition there was an increase in the residual mass at 700°C from about 0.37% for the NR-*g*-MMA to 5.13% for the silica-incorporated sample due to the presence of *in situ* silica in the composites. However, the inclusion of silica in the grafted NR does not enhance the thermal oxidative degradation of the NR composite, probably because of the low silica content.

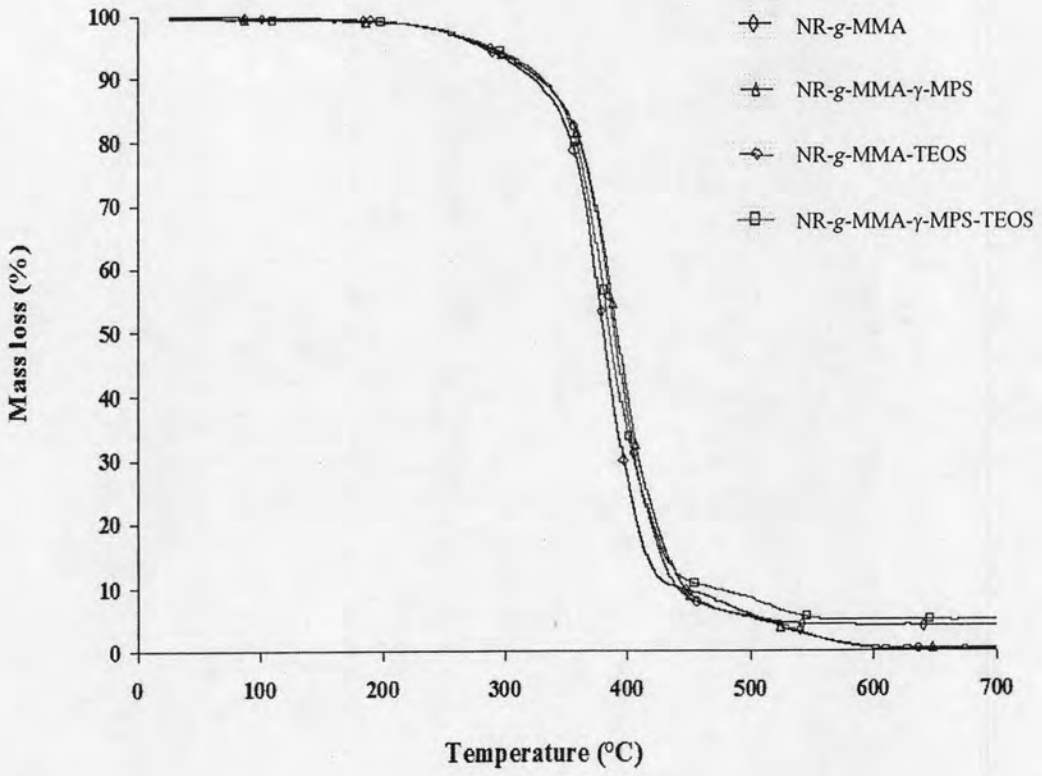

Figure 4.16 Thermo-gravimetric curves of various composite films.

Table 4.6 Results from thermo-gravimetric analysis of various composite films

Sample	Onset Temp. (°C)	Mass change (%)		Residual Mass (%) at 700°C
		25-450 (°C)	450-600 (°C)	
NR-*g*-MMA	355.8	92.36	7.27	0.37
NR-*g*-MMA-TEOS	349.7	89.73	6.28	3.99
NR-*g*-MMA-γ-MPS	356.1	92.77	6.37	0.86
NR-*g*-MMA-γ-MPS-TEOS	350.5	89.06	5.63	5.31